ACS OMEGA

Article

http://pubs.acs.org/journal/acsodf

Effect of PEGylation on Ligand-Targeted Magnetoliposomes: A Missed Goal

Joan Estelrich,*[,†,§] Maria Antònia Busquets,[†,§] and María del Carmen Morán[‡,§]

[†]Secció de Fisicoquímica; Departament de Farmàcia, Tecnologia Farmacèutica i Fisicoquímica; Facultat de Farmàcia i Ciències de l'Alimentació, [‡]Secció de Fisiologia; Departament de Bioquímica i Fisiologia; Facultat de Farmàcia i Ciències de l'Alimentació, and [§]Institut de Nanociència i Nanotecnologia UB (IN2UB), Universitat de Barcelona; Avda. Joan XXIII, 27-31, 08028 Barcelona, Catalonia, Spain

Supporting Information

ABSTRACT: We tested the targeting efficiency of magnetoliposomes (MLPs) labeled with tripeptide arginine-glycine-aspartic acid (RGD) on two types of cells: HeLa cells expressing RGD receptors and 3T3 cells lacking RGD receptors. The targeting ability of RGD-MLPs was compared to that of bare MLPs and MLPs stabilized with poly(ethylene glycol) (PEG). Cellular internalization of these liposomes was determined by flow cytometry and confocal microscopy, which showed that both types of cells took up more nontargeting MLPs than targeting RGD-MLPs or PEG-MLPs, with PEG-MLPs showing the lowest degree of internalization. The presence of specific receptors on HeLa cells did not facilitate the binding of RGD-MLPs, probably due to the presence of PEG chains on the liposomal surface. The polymer increases the circulation time of the liposomes in the organism but reduces their interactions with cells. Despite the localization of the RGD peptide on the tip of PEG in RGD-MLPs, the interaction between the liposome and cell was still limited. To avoid this drawback, targeting drug delivery systems can be prepared with two types of PEG: one of a short length to enable biocompatibility and the other of a longer chain to carry the ligand.

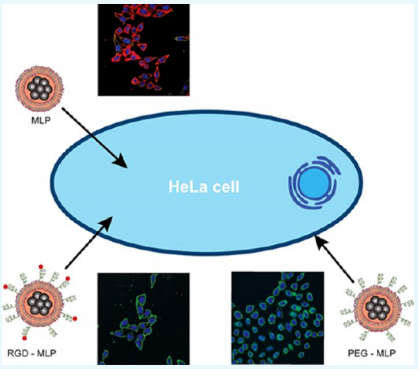

INTRODUCTION

The conventional administration of drugs presents some limitations and problems. For many treatments, large drug doses are required to achieve high local concentrations, with the potential risk of adverse side effects. Moreover, the lack of targeted delivery to the site of interest and the rapid clearance by the mononuclear phagocyte system (MPS) pose other critical challenges for the administration of any drug.[1] Recent advances in materials science and biotechnology have enabled the development of new methods of drug delivery that can potentially overcome the abovementioned limitations. One of these methods involves the use of particulate systems for drug delivery, such as microspheres, nanoparticles, lipoproteins, soluble polymers, micelles, and liposomes.[2] Targeting nanoparticles can increase the efficiency of drugs by delivering them directly to the sites of interest. This requires site-directed ligands on the surfaces of the systems to further enhance their selective targeting or the engineering of stimuli-sensitive systems that change their physical properties in response to an external stimulus (e.g., temperature, pH, ionic strength, or a magnetic gradient for magnetic targeting).[3]

Magnetic nanoparticles (MNPs) are promising stimuli-sensitive drug carriers because of their responsiveness to a magnetic field. An applied extracorporeal magnetic field can concentrate these nanosystems at the desired site, keeping them in a particular place for a given period of time until the encapsulated drug is released, thereby minimizing any side effects due to nonspecific distributions.[4−6]

Ligands (e.g., antibodies, peptides, or carbohydrates) recognizing tumor-associated antigens expressed on tumor cell surfaces have been used for cancer therapy. Some of the structures suitable for tumor targeting belong to integrins, a family of heterodimeric cell surface receptors, consisting of α- and β-subunits, which mediate cell adhesion to the extracellular matrix and other cells.[7] These cell surface receptors are universally expressed by tumor and normal cells. However, the α_V (especially $\alpha_V\beta_3$) forms are highly expressed on endothelial cells lining tumor cells but poorly expressed on resting endothelial cells and most normal organs, making them a potential target for antiangiogenesis treatment. Targeting the $\alpha_V\beta_3$ integrin may provide an opportunity to targeting the tumor endothelium and destroy tumor vessels without harming the microvessels of normal tissue.[8] Indeed, targeting tumor vasculature rather than the tumor cells themselves has been described as a promising new approach for cancer therapy.[9] The ligands that have been used for targeting these integrins carry the arginine-glycine-aspartic acid (RGD) motif. The RGD sequence forms the basis of a variety of RGD-containing peptides that

Received: June 16, 2017
Accepted: July 31, 2017
Published: October 9, 2017

DOI: 10.1021/acsomega.7b00778
ACS Omega 2017, 2, 6544−6555

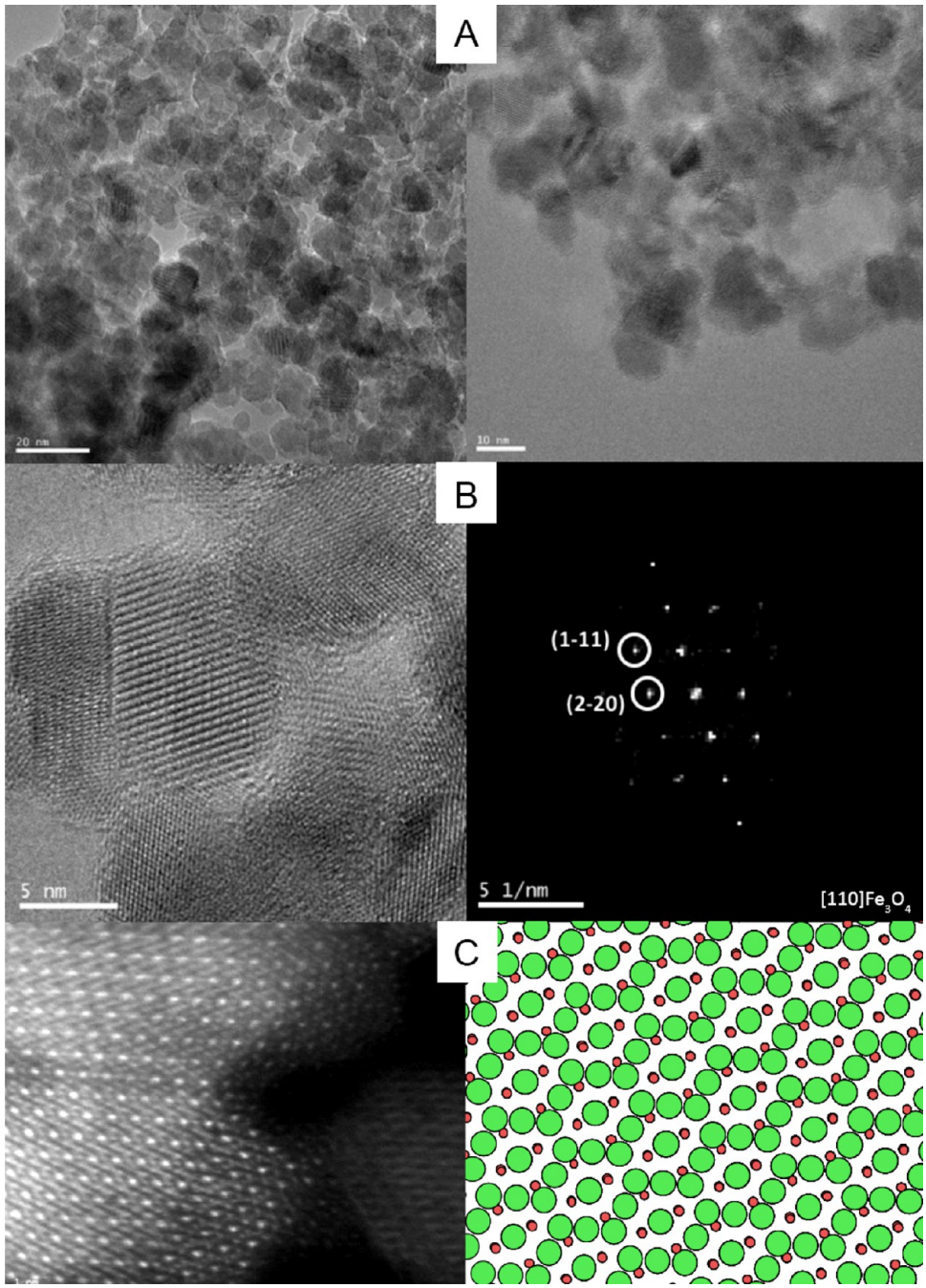

Figure 1. Characterization of iron oxide nanoparticles: (A) TEM images; (B) HRTEM image and fast Fourier transform (FFT) from the highlighted region; and (C) HAADF image of the sample. The right panel is the crystal model of magnetite seen along the [110] zone axis, which matches with the highlighted region of the image.

display preferential binding to either the $\alpha_V\beta_3$ integrin and related α_V integrins or other types of integrins. Because the RGD sequence is conserved in all natural and newly developed ligands, the relative affinity and specificity of the peptides and proteins are determined by other amino acid residues flanking the RGD motif, especially the two amino acids following the aspartic acid.[10] In addition to the direct interactions between these residues and integrin, flanking groups influence the folding of the peptide and thus its conformation. Cyclization is commonly used to improve the binding properties of RGD peptides.[11] Linear RGD peptides are highly susceptible to chemical degradation due to the reaction of the aspartic residue with the peptide backbone.[12] Because the rigidity conferred by cyclization prevents this problem, cyclic peptides are more stable and suitable for biological targeting. Thus, RGD-containing peptides have been used in tumor imaging, treatments against angiogenesis, and tumor targeting with radionuclides or chemotherapeutic drugs.[13]

Liposomes have been extensively investigated as potential drug carriers in cancer chemotherapy.[14] A major drawback of using liposomes is their rapid degradation by the mononuclear phagocyte system (MPS). As with all foreign colloidal particles, liposomes are quickly recognized as "nonself" and taken up by the cells of the MPS, chiefly macrophages in the liver and spleen. To prolong their circulation time in vivo, poly(ethylene glycol) (PEG) is grafted onto the lipid surface.[15] Such liposomes,

DOI: 10.1021/acsomega.7b00778
ACS Omega 2017, 2, 6544−6555

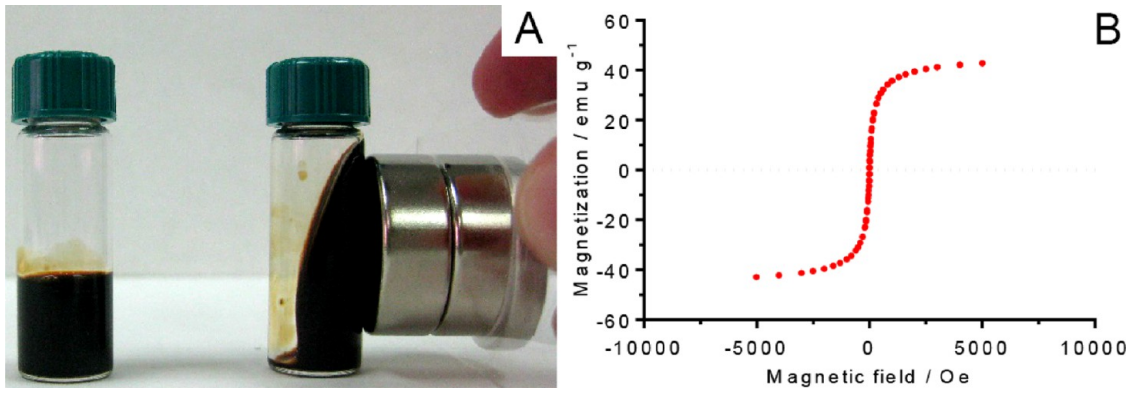

Figure 2. (A) Effect of an external magnet on the ferrofluid. (Photograph courtesy of J. Estelrich Copyright 2016) (B) Magnetization measurement at 298 K of a sample of lyophilized ferrofluid.

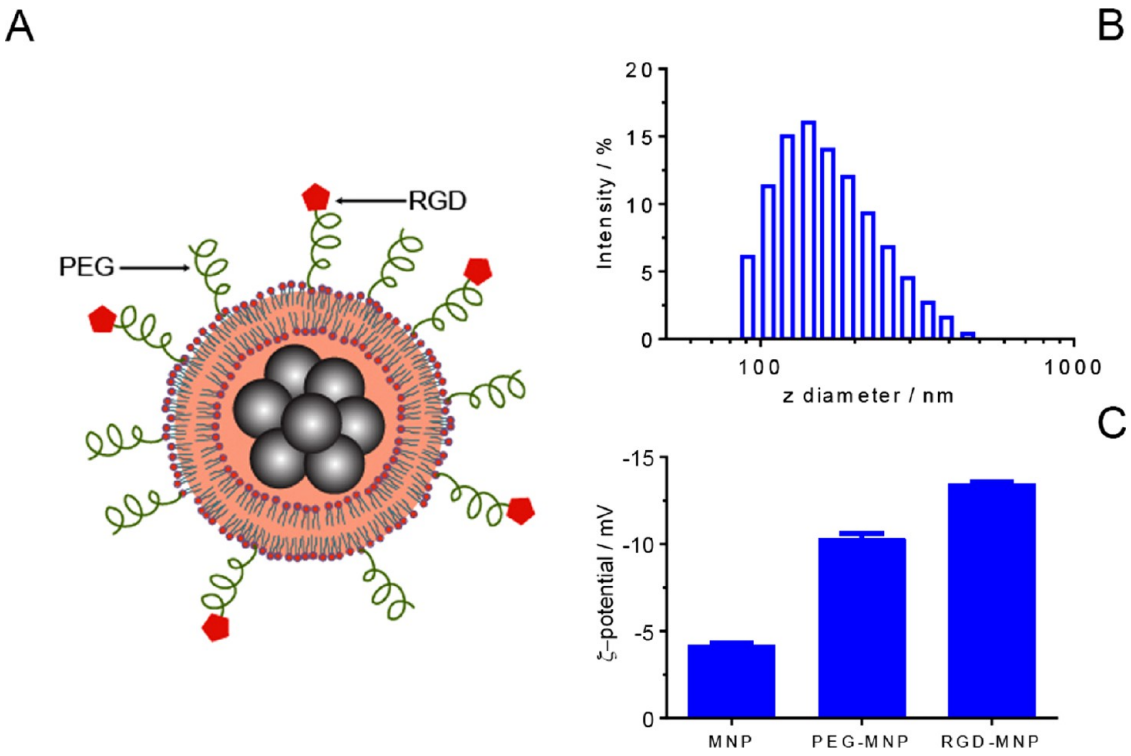

Figure 3. Characterization of magnetoliposomes (MLPs): (A) schematic diagram of the structure of a RGD-MLP; (B) hydrodynamic diameter distribution for MLPs, PEG-MLPs, and RGD-MLPs diluted in water; and (C) ζ-potentials of MLPs, PEG-MLPs, and RGD-MLPs diluted in 10^{-4} M KBr.

classified as sterically stable liposomes, present a hydrophilic corona around the particles that minimizes nonspecific adsorption of proteins onto the liposome surface, thus rendering the liposomes "invisible" to macrophages ("stealth" effect). Liposomes smaller than 200 nm can exploit a feature of the tumor microenvironment, the so-called enhanced permeability and retention (EPR) effect.[16] Because of the leaky vasculature of the tumor, the intratumoral accumulation of liposomes is high relative to normal tissue.[17,18]

In this study, magnetoliposomes (MLPs) and sterically stabilized liposomes containing magnetic nanoparticles (PEG-MLPs) were prepared. Such liposomes can be targeted to the site of interest by applying an external magnetic field. To generate RGD-MLPs, the RGD peptide was grafted onto the distal end of the PEG chain attached to the liposomes to target integrin $\alpha_V\beta_3$ expressed on many cancer cells. Hence, this kind of liposome (RGD-MLPs) combines magnetic and receptor-specific targeting. The targeting efficiency of RGD-MLPs in vitro was tested on two types of cells: 3T3 murine Swiss albino embryo fibroblasts and HeLa cells derived from human epithelial cervical cancer. We selected these cell lines from different species and with different embryonic origins as model systems to understand the cell-specific responses induced by our nanoparticles.[19]

Cellular uptake of RGD-MLPs, MLPs, and PEG-MLPs was studied in 3T3 and HeLa cells after establishing the safe working concentrations of these liposomes for cell labeling. To visualize the cellular uptake of the liposomes by confocal microscopy and flow cytometry, liposomes were prepared by incorporating 0.3 mol % rhodamine B (Rho) into the lipid bilayer.

DOI: 10.1021/acsomega.7b00778
ACS Omega 2017, 2, 6544−6555

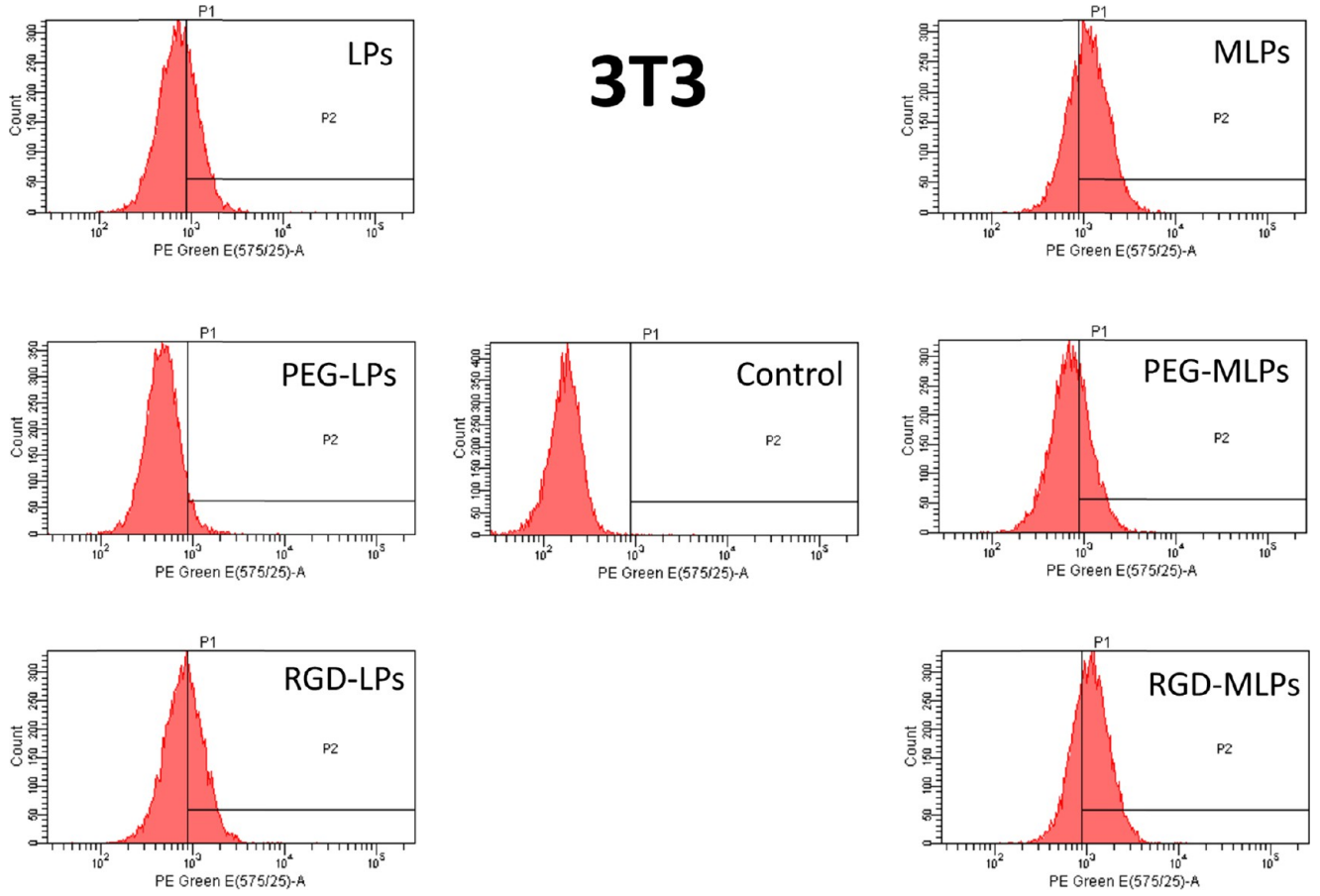

Figure 4. Flow cytometry histograms of 3T3 cells incubated for 4 h with MLPs, PEG-MLPs, or RGD-MLPs and their nonmagnetic counterparts. In the center, the fluorescence of untreated cells is shown.

RESULTS

Characterization of MNPs and RGD-MLPs. MNPs were synthesized by coprecipitating iron salts in the presence of PEG. The resulting ferrofluid was characterized by transmission electron microscopy (TEM), high-resolution TEM (HRTEM), high-angle annular dark-field imaging (HAADF), (Figure 1) photon correlation spectroscopy (PCS), and Doppler microelectrophoresis.

From the TEM images, we can observe that the ferrofluid consisted of small clusters of primary particles with diameters between 5 and 15 nm (Figure 1A). Figure 1B displays a HRTEM image of the iron oxide nanoparticle sample. The appearance was that of ultrafine agglomerate crystallites. The two distinct levels of contrast indicate that nanoparticles contained several components. The FFT of the labeled squared region showed the diffraction pattern of magnetite in the [112] zone axis. The HAADF image (Figure 1C) showed the nanoparticles at atomic resolution. The right panel is the crystal model seen along the [110] zone axis, which matched with the highlighted region of the image. PEG-coated magnetic nanoparticles had an intensity-weighted average hydrodynamic diameter of 62 ± 13 nm with a polydispersity index (PI) of 0.10 ± 0.06 from PCS measurements. The hydroxyl groups of the PEG were responsible for the low surface charge of the nanoparticles at pH 6.5 (ζ-potential ~5 mV). The particles responded to an external magnetic field (Figure 2A), exhibited superparamagnetic behavior, and had a magnetization of 55 emu g^{-1} at 5 kOe at room temperature (Figure 2B). The colloidal stability of the ferrofluid under perikinetic conditions was extremely high; the size and size distribution remained unaltered for more than 5 years. This ferrofluid was encapsulated in bare and PEGylated liposomes. One part of the PEGylated liposomes was functionalized with the RGD peptide at a ratio of 1:10 RGD/PEG. For flow cytometry and confocal microscopy, fluorescence probe Rho was inserted into MLPs at a ratio of 100:3 lipid/Rho.

Figure 3 shows the main characteristics of these MLPs. Figure 3A is a schematic representation of the functionalized MLPs. The average hydrodynamic diameter was 220 ± 4 nm for MNPs, 146 ± 4 nm for PEG-MNPs, and 161 ± 0.5 nm for RGD-MNPs (Figure 3B). The size distribution of all of the MLPs was monomodal (PI ~ 0.20). Electrophoretic mobility measurements of MLPs, PEG-MLPs, and RGD-MLPs indicated ζ-potentials of −4.2 ± 0.1, −10.3 ± 0.3, and −13.5 ± 0.1 mV, respectively (mean ± standard deviation) (Figure 3C). The iron content, determined spectroscopically, was 10 mM. This amount, in relation to the phospholipid concentration of 25 mM, corresponded to 23.52 mg of iron by millimole of phospholipid.

The lipids present in the liposome membrane have the following molecular surface areas: 0.62 nm^2 for dimyristoyl phosphatidyl choline (DMPC),[20] 0.48 nm^2 for distearoyl phosphatidyl ethanolamine (DSPE),[21] and 0.35 nm^2 for cholesterol (CHOL).[22] From the molar ratio of RGD-MLPs and taking into consideration a symmetrical distribution of lipids in the bilayer and ideal mixing, where the area per molecule is simply a weighted average of the pure component areas, an average lipid molecular surface area of 0.514 nm^2 was calculated.

DOI: 10.1021/acsomega.7b00778
ACS Omega 2017, 2, 6544−6555

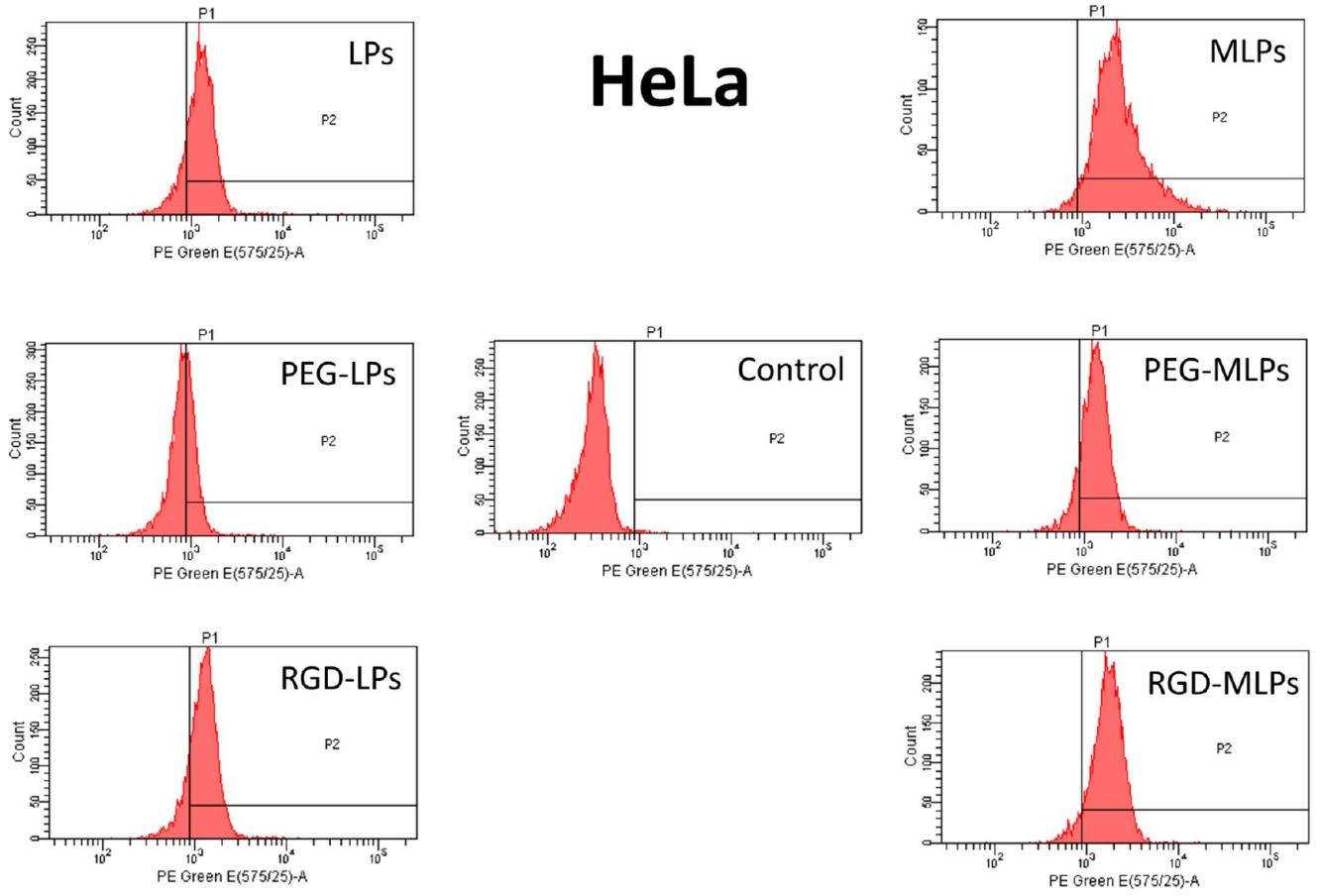

Figure 5. Flow cytometry histograms of Hela cells incubated for 4 h with MLPs, PEG-MLPs, or RGD-MLPs and their nonmagnetic counterparts. In the center, the fluorescence of untreated cells is shown.

Assuming a liposome diameter of 100 nm and that all of the RGD motifs present were coupled to a maleimide group (this reaction has been reported to be one of the most efficient reactions in bioconjugate chemistry),[23] the number of RGD molecules present in the outer monolayer of the liposomes was ∼180. The average number of iron oxide cores in the liposomes was calculated to be 1.35, which is consistent with the inner volume of a liposome as well as the hydrodynamic radius of a magnetic particle. For this calculation, the iron oxide cores were assumed to be monodispersed (12 nm in diameter), perfectly spherical, and with a density of 5100 kg m^{-3}.

Cell Viability. Before studying the cellular internalization of MLPs, safe working concentrations of the three types of MLPs were first established. The effects of targeting RGD-MLPs on HeLa and 3T3 cells were evaluated and compared to those of nontargeting MLPs and PEG-MLPs. First, the cytotoxic effects exerted by the ferrofluid and bare liposomes were determined. It is known that iron oxide nanoparticles can be internalized into cellular compartments, such as the lysosome, and that permeabilization of the lysosome membrane promotes cell death.[24] We observed that after 24 h of incubation the ferrofluid did not affect the cell cycle in the range of 0.05−12 mM Fe, as determined by the neutral red (NR) uptake assay.

The half-maximal inhibitory concentration (IC_{50}) of the ferrofluid in both cell types was >12 mM (Table S1 and Figure S1). The range of safe concentrations was lower in the 3-(4,5-dimethylthiazol-2-yl)-2,5-diphenyltetrazolium bromide (MTT) assay. In the 0.05−0.20 mM range, the iron oxide cores themselves did not exert toxic effects on the cells. IC_{50} values of 5.6 and 8.4 mM were obtained in 3T3 and HeLa cells, respectively. To determine any potential toxic effects of the liposomes, cell viability was assessed in the presence of bare liposomes, that is, liposomes formed solely of DMPC and CHOL at the same molar ratio as that used to prepare the three types of MLPs studied here. This lipid composition was completely innocuous (IC_{50} > 20 mM) (Table S1 and Figure S2). To study the toxicity of the three types of MLPs, cells were exposed to a concentration range of nanoparticles (0.08−20 mM) for 24 h. These nanoparticles induced some toxicity at relatively high concentrations, especially those containing PEG (Table S1 and Figures S3−S5). On the basis of these results, subsequent experiments were performed using a phospholipid concentration of 0.60 mM (with an iron content of 0.2 mM).

Flow Cytometry. Flow cytometry was used to determine the relative amount of intracellular uptake of the different MLPs. Forward and sideward scatter diagrams of single-cell suspensions demonstrated that at least the majority of cells were still intact, with only small amounts of debris occurring (Figures S6 and S7). To distinguish between fluorescence caused by MLP binding and autofluorescence from unlabeled cells, the autofluorescence of cells was measured and a cutoff point was determined. After incubation of 3T3 and HeLa cells with MLPs, PEG-MLPs, or RGD-MLPs for 4 h, flow cytometry revealed significantly higher mean fluorescence intensities for cells incubated with MLPs (regardless of their composition) compared to those for control cells (Figures 4 and 5). Both endpoints emphasize different properties of the cell. Whereas MTT measures the mitochondrial activity, NR gives information about the membrane integrity. In

DOI: 10.1021/acsomega.7b00778
ACS Omega 2017, 2, 6544−6555

addition, NR has to be accumulated in lysosomes for staining and changes in lysosomal function/pH can cause decreased dye uptake. Therefore, uptake of particles, for instance, could cause the changes in lysosome pH. However, only in the case of ferrofluid (see Figure S1), a strong influence of the endpoint method on the selectivity on the mode of action was observed. Changes in cell viability determined by these two endpoints suggested that the interaction of ferrofluid with cells involves a poor interaction with the plasmatic membrane. The bare and PEGylated MLPs (Figure S3) did not demonstrate so strong differences between these systems. In both cases, the decrease in cell viability using MTT suggested the uptake and internalization mediated by the nanoparticulated system.

In 3T3 cells, MLP uptake increased the mean fluorescence intensity by a factor of 6−7, whereas RGD-MLPs and PEG-MLPs produced a fluorescence signal 6 and 4 times stronger, respectively. The differences in fluorescence intensities between MLPs and the other two liposomes were greater in HeLa than in 3T3 cells. In this way, MLPs increased the mean fluorescence intensity by a factor of 8−9 in HeLa cells, with the fluorescence intensity being only 5 times stronger with RGD-MLPs and 4 times stronger with PEG-MLPs. To ascertain whether the magnetic properties of the liposomes affected cellular uptake, the uptake of bare liposomes with no ferrofluid was also studied. In 3T3 and especially HeLa cells, MLPs were internalized to a higher extent than in bare liposomes. Table 1 summarizes the results.

Table 1. Fluorescence (Mean and Increase) Observed for Cells Incubated with MLPs with Respect to Control Cells

	cell line			
	Hela		3T3	
liposome type	F/F^o	mean	F/F^o	mean
MLP	8.46	1339	6.43	818
PEG-MLP	4.06	866	4.17	511
RGD-MLP	5.26	1327	6.13	904
bare liposome	3.83	3231	4.13	1272
PEG-liposome	2.48	1407	2.70	843
RGD-liposome	3.83	1829	4.54	1235
control	1.00	331	1.00	186

Confocal Microscopy. To visualize the distribution of the fluorescence signals in cells, laser scanning confocal microscopy was performed with 3T3 and HeLa cells (Figures 6−9) after 2, 4, and 24 h of incubation with any of the types of MLP bearing Rho (red channel). The cell membrane was stained with cell-membrane-impermeable dye Alexa Fluor 488-conjugated wheat germ agglutinin (WGA) (green channel), whereas the nucleus was stained with membrane-permeable dye Hoechst 33342 (blue channel). Figure 6 shows the negative control of both 3T3 and HeLa cells.

Figures 7 and 8 show representative confocal images of the cells incubated for 2, 4, or 24 h with bare MLPs (Figure 7) or RGD-MLPs (Figure 8). Figure 9 shows the representative confocal images of the cells incubated with PEG-MLPs. Images obtained from the red and green channels were merged. After internalization, nanoparticles are initially confined inside endosomes, which are submicrometric vesicles of the endocytic pathway. Internalization of nanoparticles into endosomes is indicated by the red liposome fluorescence between the green cell membrane and the blue nucleus in the confocal images, which is absent in the images of corresponding control cells. Figure 7A shows that MLP internalization in 3T3 cells after 24 h of incubation is greater. In HeLa cells (Figure 7B), MLP internalization could already be observed at 2 h but became lower at 24 h. Thus, the kinetics of nanoparticle uptake depended on the type of cell and it is particularly fast. RGD-MLP internalization could be clearly seen in 3T3 cells at 2 and 4 h of incubation, but only a few cells displayed uptake after 24 h (Figure 8A). By contrast, HeLa cells did not internalize RGD-MLPs at any of the time points studied (Figure 8B). The internalization of PEG-MLPs was unappreciable at any incubation time (Figure 9A,B). These results were consistent with those obtained with flow cytometry.

DISCUSSION

Adding specific ligands to the surfaces of nanoparticles to target receptors that are overexpressed in anomalous circumstances in cells (e.g., the overexpression of $\alpha_V\beta_3$ integrin or CD44 in cancerous cells) is a good strategy for concentrating nanoparticles at the sites of interest and, thus, facilitating their internalization and accumulation inside the desired cells via the EPR effect. Moreover, nanoparticles can carry a drug and release it more efficiently inside the cells of interest. Nanoparticles can

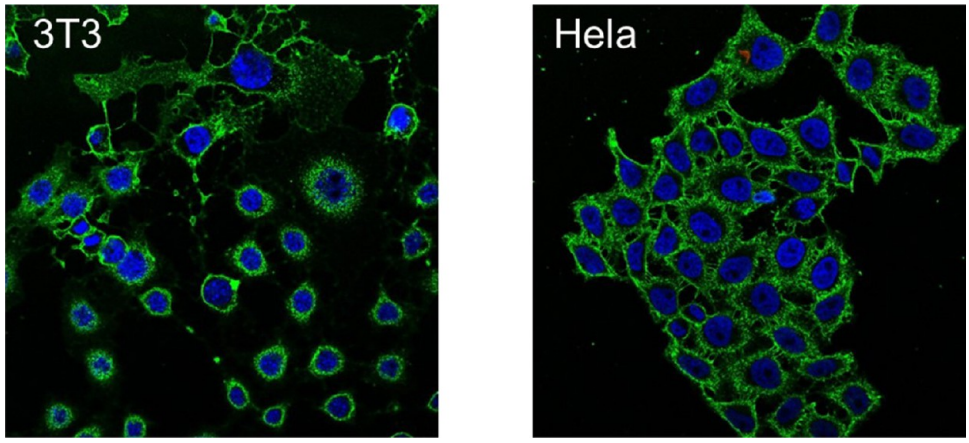

Figure 6. Confocal microscopy images of the cells incubated without nanoparticles for 4 h. Green fluorescent signals indicate the cellular membranes, and the blue ones, the nucleus.

DOI: 10.1021/acsomega.7b00778
ACS Omega 2017, 2, 6544−6555

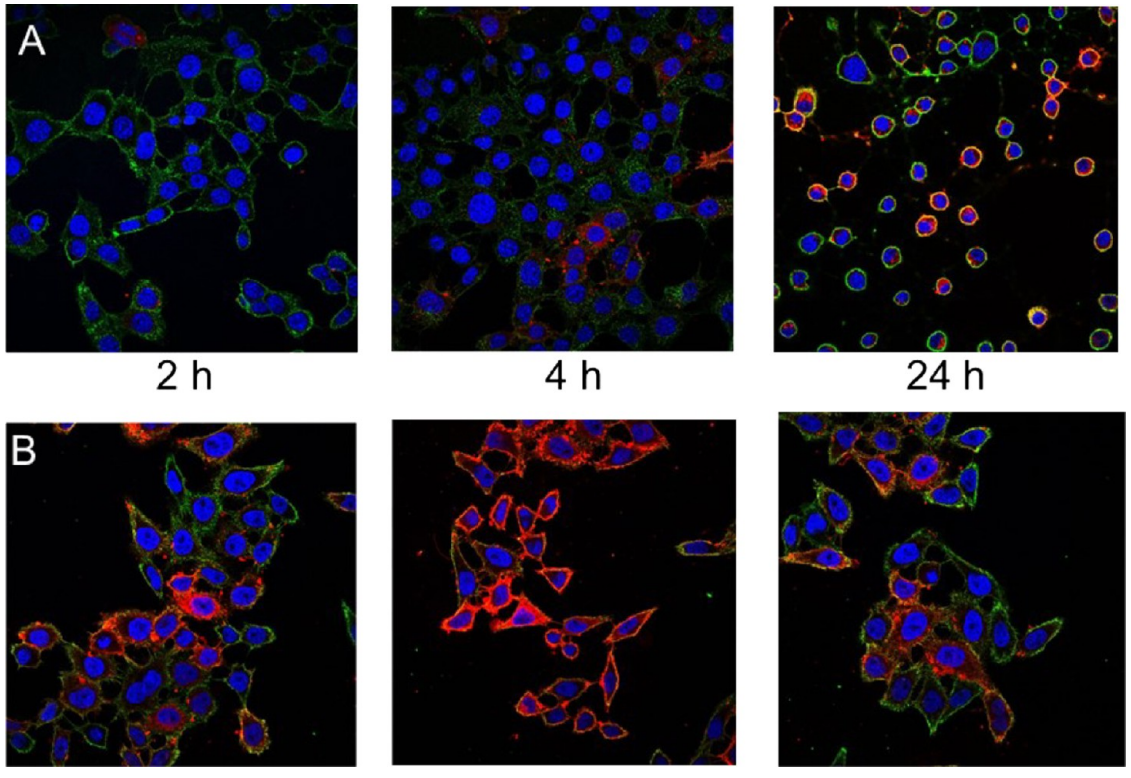

Figure 7. Confocal microscopy images of the intracellular distribution of MLPs after three times of incubation (2, 4, and 24 h). Green fluorescent signals indicate the cellular membranes, blue signals, the nucleus, and red signals, the nanoparticles: (A) 3T3 cells and (B) HeLa cells.

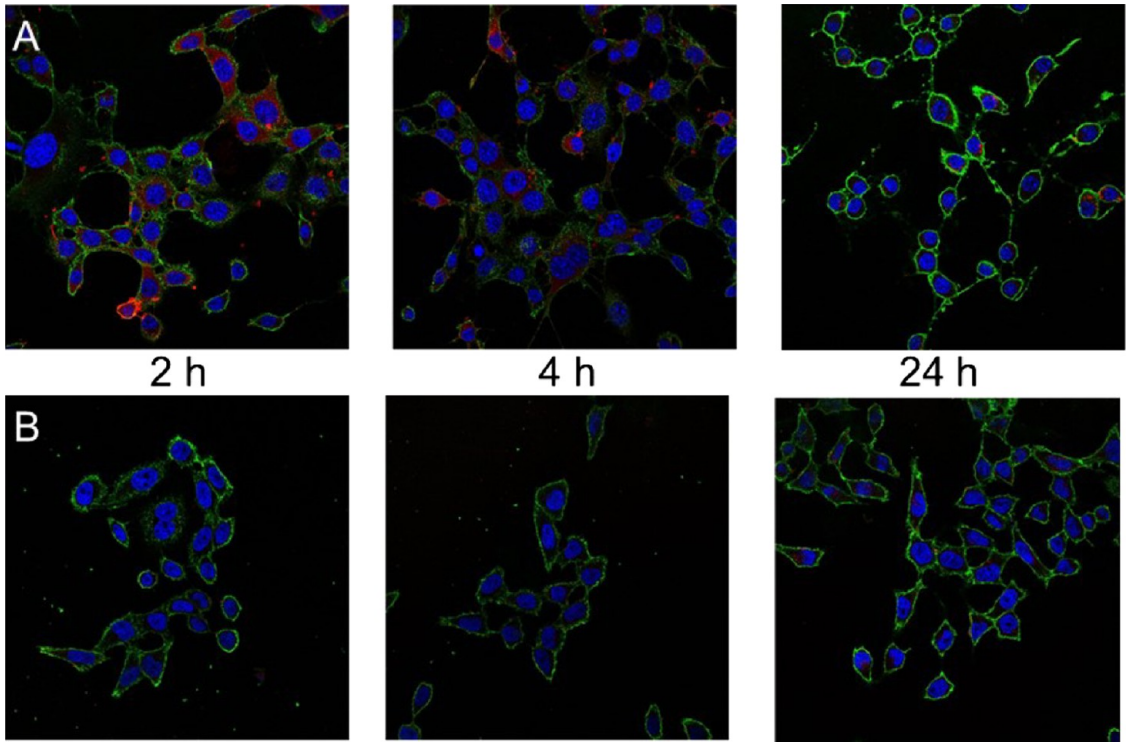

Figure 8. Confocal microscopy analysis of the intracellular distribution of RGD-MLPs after three times of incubation (2, 4, and 24 h). Green fluorescent signals indicate the cellular membranes, blue signals, the nucleus, and red signals, the nanoparticles: (A) 3T3 cells and (B) HeLa cells.

also contain iron oxide cores conferring superparamagnetic properties of a suitable size. Such nanoparticles can be used to induce death of the cells in the vicinity by generating heat after exposure to radiofrequency radiation (hyperthermia) or to visualize pathological conditions by magnetic resonance imaging. In conclusion, it is possible to prepare nanoparticulate systems that behave as multifunctional nanoplatforms. Among the different types of nanoparticles that can be used as theranostic

DOI: 10.1021/acsomega.7b00778
ACS Omega 2017, 2, 6544−6555

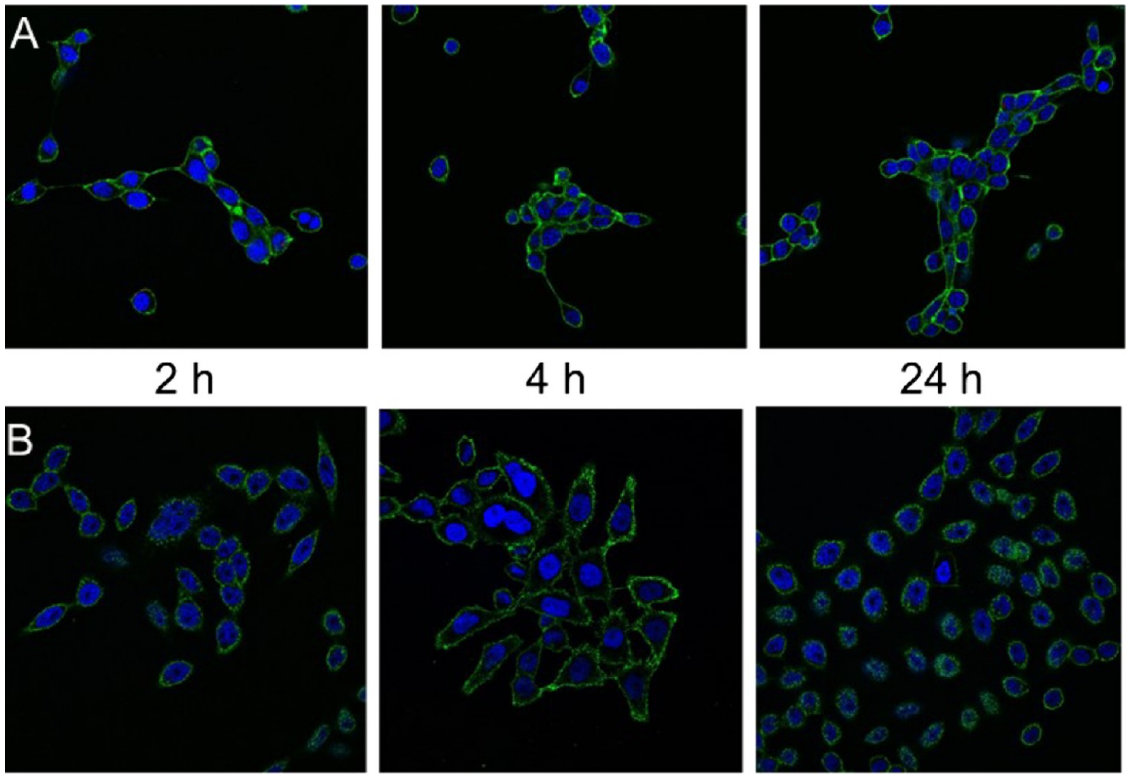

Figure 9. Confocal microscopy analysis of the intracellular distribution of PEG-MLPs after three times of incubation (2, 4, and 24 h). Green fluorescent signals indicate the cellular membranes, blue signals, the nucleus, and red signals, the nanoparticles: (A) 3T3 cells and (B) HeLa cells.

platforms, targeted MLPs are a good example. Indeed, a wide range of ligand-bearing MLPs (or liposomes) have been described to date.[9,25−30]

In the present work, functionalized MLPs bearing RGD moieties were used for the specific labeling of $\alpha_V\beta_3$-integrin-expressing HeLa cells and for the unspecific labeling of 3T3 fibroblasts (which also present integrins on their surface but are collagen receptors and not RGD receptors).[31] The cell interactions of the RGD-MLPs were compared to those of RGD-lacking MLPs (with or without PEG).

We first prepared iron oxide nanoparticles stabilized with PEG, which is currently considered to be the best antibiofouling agent and described as GRAS (generally regarded as safe) by the U.S. Food and Drug Administration. The ferrofluid was encapsulated in bare liposomes and in liposomes with PEG attached covalently to the lipid surface. Furthermore, a part of the PEGylated liposomes was functionalized with cyclic peptide RGD to generate RGD-MLPs. The average diameter of the obtained MLPs was lower than 220 nm (≈the pore size of the membranes used). The reduction of size in all types of the prepared liposomes was due to the presence of CHOL because it produces a condensation effect resulting from particular changes in the phase behavior elicited by CHOL.[32] Moreover, compared with MLPs, PEG-MLPs and RGD-MLPs presented a significantly lower diameter due to the insertion of PEG. PEG affects compressibility and the packing of the lipid bilayer, with PEG-DSPE concentrations higher than 8 mol % decreasing the particle size due to the appearance of PEG-DSPE-enriched micelles at the expense of liposomes.[33] Regarding the number of iron oxide cores inside the liposomes, the theoretical value of 1−2 cores per liposome is consistent with the inner volume of an average liposome (with a diameter of 150 nm) and the hydrodynamic radius of a nanoparticle of ferrofluid because the high hydrophilicity of PEG involves a high level of hydration of the polymer.

Historically, iron oxide nanoparticles have been considered safe given the high levels of iron ions that can be tolerated (up to 4 mM). However, some groups have more recently shown that exposure to iron oxide nanoparticles can lead to a wide variety of toxic effects impacting the cell morphology, cytoskeleton, proliferation, viability, and cellular homeostasis.[34−37] Our results showed that the MLPs used in this study were not toxic to 3T3 and HeLa cells, when using the NR assay (IC_{50} > 12 mM). This value was lower for the MTT assays, which measure levels of mitochondrial dehydrogenase enzymes (Figure S1, Supporting Information). Our data indicated that bare liposomes and MLPs were innocuous up to a lipid concentration of 10 mM after 24 h of incubation (Table S1 and Figures S2 and S3). By contrast, RGD-MLPs and PEG-MLPs exhibited an appreciable toxicity that differed in its extent between the 3T3 and HeLa cells (Figures S4 and S5). For instance, RGD-MLPs, at a lipid concentration of 0.6 mM, reduced cell viability to 73.2 ± 5.6% in 3T3 cells and 81.4 ± 3.6% in HeLa cells (in the MTT assays). At the same concentration, bare MLPs and bare liposomes gave cell viabilities of ca. 100% in 3T3 and HeLa cells for both the NR and MTT assays. As a control, there were no cytotoxic effects when identical volumes of a nanoparticle-free buffer were used to replace the medium, indicating that the reduction in cell viability was not due to a limited nutrient supply.[38] The toxic effects could be attributed to any of the components present in the liposome (e.g., the maleimide group or the cyclic peptide). Although a lack of toxicity of liposomes bearing the maleimide group has been shown previously,[39] the toxicity of both RGD-MLPs and PEG-MLPs could be due to the cyclic peptide promoting the toxicity elicited by the maleimide group.

DOI: 10.1021/acsomega.7b00778
ACS Omega 2017, 2, 6544−6555

Our flow cytometry results were initially quite surprising. MLPs, regardless of their composition, were internalized to a greater extent than the nonmagnetic liposomes in both cell lines (Table 1). For instance, the increase in the mean fluorescence intensity produced by MLPs was more than twice (8.46 vs 3.83) that obtained with bare liposomes in HeLa cells. Not less surprising, PEGylated liposomes (with or without iron oxide nanoparticles) produced the lowest values for cell binding. Although all of the systems become aggregated as a consequence of their interaction with the media components, the kinetics of the aggregation is different, and for that reason, the MLPs are probably taken up quicker than the functionalized samples. Internalization of these nanoparticles was investigated by confocal microscopy, and the results were wholly consistent with those obtained with flow cytometry. Figures 7 and 8 demonstrate that time was a key factor in the internalization process; the highest degree of internalization of MLPs in HeLa cells was seen at 4 h of incubation, whereas the highest internalization in 3T3 cells was observed at 24 h. After internalization, nanoparticles are initially confined inside endosomes, which are submicrometric vesicles of the endocytic pathway.[40,41] Therefore, the red areas in Figure 7 show MLPs that have been internalized into endosomal compartments. RGD-MLPs were poorly internalized in 3T3 cells and not at all in HeLa cells at any of the time points examined. These results supported our flow cytometry data but are not in line with most of the other studies on RGD.[9,26,29,42,43] The absence of RGD-MLP internalization could be because RGD-MLPs remain primarily linked to the cell surface, with the repeated washes performed before the microscopic experiments causing the nanoparticles to detach from the cell surface. Previous studies have demonstrated that nanoparticle internalization in HeLa lines strongly depends on the nanoparticle coating charge, nature, concentration, and incubation time.[44,45] Thus, nanoparticles with low surface charge or negative charge are hardly endocytosed by these cells, partly explaining the lack of internalization of RGD-MLPs, which display a low surface charge. By contrast, cationic nanoparticles were detected inside the cells under all experimental conditions.

We observed greater internalization of MLPs than that of their nonmagnetic counterparts, the reasons for which remain unclear. The extremely low cellular uptake of RGD-MLPs (or RGD-liposomes) in HeLa cells despite the specific targeting could be explained by the presence of PEG. PEGylation has been, for many years, used to avoid the interaction between any carrier and the components of biological fluids. Although PEGylated carriers are effectively delivered to tumor tissue via an EPR effect, the cellular uptake efficiency of PEGylated carriers is known to be low. This problem is recognized as the PEG dilemma.[46−48] It has been shown that PEGylation diminishes the absolute amount of protein bound to the liposomes but does not impede the formation of the protein layer surrounding the liposome (the protein corona).[49] To overcome this drawback and enhance the cellular uptake efficiency of PEGylated carriers, ligands targeting surface proteins on cancer cells have been attached to the tip of PEG.[50,51] The aim of our study was to facilitate and increase the cellular uptake of nanoparticles by incorporating RGD. However, as we have demonstrated, RGD-MLP internalization was almost similar to the uptake of their PEGylated counterparts despite the presence of the ligand. It is evident that these PEGylated systems, with longer circulation time in the bloodstream, interact inefficiently with cell membranes. In other words, when PEG is attached to the liposomal surface, the designed active targeting is masked. Therefore, it is necessary to find the best compromise between an antiopsonization strategy and efficient cellular uptake because an optimal balance between PEGylation and RGD loading is required for targeting in vivo. In some cases, higher RGD loading could be applied to increase cell binding (or similarly, a reduction in PEGylation could be used to increase binding), whereas in others, the use of ligand-targeted liposomes without PEG or with a shorter-chain PEG could be a reasonable strategy.[52]

CONCLUSIONS

The cellular uptake of MLPs is strongly related not only to the surface grafting of the nanoparticle but also to the presence of encapsulated iron nanoparticles. While PEGylation inhibits internalization, the targeting RGD moiety does not favor internalization, even in cells with RGD receptors. Furthermore, bare MLPs are internalized more than the other types of MLPs, regardless of the cell type. Therefore, the cellular uptake of ligand-targeted MLPs is inhibited by PEG. To achieve cell interaction and internalization of targeting nanoparticles, their surfaces have to display ligands that exceed the length of the polymer chain to prevent the protein corona impeding the binding ability of the ligand. However, it seems more straightforward to use two PEG chains of different lengths.[53,54] The short PEG chains afford the steric stability of the nanoparticles, whereas the longer ones help locating the ligand. Consequently, the long arm facilitates the interaction with the cellular receptor, whereas the short arm prevents the adsorption of proteins on the particles' surface. In this way, the ligands must be attached at the tip of a PEG chain longer than the PEG chains used to provide steric stabilization.

Experimental Procedures. Synthesis and Characterization of Magnetoliposomes. Iron oxide magnetic ferrofluid was synthesized by coprecipitating two iron salts in the presence of PEG with a molecular weight of 6000 Da, as described by García-Jimeno and Estelrich.[55] MLPs were prepared with DMPC (P7930, Sigma-Aldrich, St. Louis, MO) and CHOL (C8667, Sigma-Aldrich) at an 80:20 molar ratio. PEG-MLPs were made with DMPC, CHOL, and DSPE-PEG2000 (880160P, Avanti Polar Lipids, Alabaster, AL). RGD-MNPs were prepared with DMPC, CHOL, and DSPE-PEG2000 (880160P, Avanti Polar Lipids), as well as maleimide-PEG-DSPE (DSPE-PEG-MAL) (880126P, Avanti Polar Lipids), and modified with RGD. The cyclic RGD peptide (Arg-Gly-Asp-D-Phe-Cys, purity assayed by HPLC to be >99%) was obtained from Caslo (Lyngby, Denmark). Lipids used either for MNPs or for RGD-MNPs were dried by evaporating at reduced pressure (Rotovapor R-200, Buchi, Switzerland) at 40 °C. The obtained lipid films were hydrated with a suspension of ferrofluid in water at an iron concentration of 0.67 mg/mL (12 mM). Liposomes were obtained by sequential extrusion through polycarbonate membranes with pore sizes of 800 nm (3 times), 400 nm (3 times), and 200 nm (4 times) in an Extruder device (Avestin, Ottawa, Canada). The nonencapsulated ferrofluid was separated from MLPs by adding an equal volume of 320 mM NaCl. The nonincorporated ferrofluid was precipitated by gentle centrifugation at 2000 rpm for 5 min. The supernatant contained the purified MLPs. RGD-MLPs were prepared similarly: DMPC/CHOL/DSPE-PEG-MAL were mixed at molar ratios of 80:20:3 and hydrated with a suspension of the ferrofluid. Once the liposomes were extruded and purified, RGD dissolved in water was coupled to the corresponding liposomal surface by a chemical reaction at room temperature overnight between the

DOI: 10.1021/acsomega.7b00778
ACS Omega 2017, 2, 6544−6555

maleimide groups at the distal end of DSPE-PEG-MAL on the liposomes and the sulfhydryl group of cysteine in the cyclic RGD, at a molar ratio of 1:10 (RGD/maleimide).[27] To determine the cellular uptake of liposomes by confocal microscopy and flow cytometry, liposomes were labeled with fluorescence probe 1,2-dimyristoyl-*sn*-glycero-3-phosphoethanolamine-*N*-(lissamine Rho sulfonyl) (ammonium salt) (810157C, Avanti Polar Lipids). The probe in chloroform/methanol (2:1, v/v) was added to the organic lipid mixture and proceeded as indicated above. The microscopic images were acquired in probe-corrected Jeol ARM-200 equipped with a field emission gun electron source operating at 200 kV. Z-contrast images were collected using an HAADF detector, in scanning transmission mode (STEM). Particle size distribution and ζ-potential were determined by PCS using Zetasizer Nano (Malvern, U.K.). The magnetic properties of the magnetic particles were evaluated using a superconducting quantum interference device magnetometer (Quantum design MPMS XL). Phospholipid and iron concentrations in the liposomal samples were determined by the Steward[56] and Kiwada[57] methods, respectively.

Cell Culture. The 3T3 (murine Swiss albino embryo fibroblasts) and HeLa (human epithelial cervical cancer) cell lines were obtained from Eucellbank (Universitat de Barcelona). Cells were routinely cultured in 75 cm^2 culture flasks and grown in Dulbecco's modified Eagle's medium (DMEM) (56499C, Sigma-Aldrich) supplemented with 10% (v/v) heat-inactivated fetal calf serum (FCS) (10082, Invitrogen), 4.5 g/L glucose, 2 mM L-glutamine, 100 U/mL penicillin, and 100 mg/mL streptomycin ("complete medium") at 37 °C and 5% CO_2. After cells became ∼80% confluent, they were removed from the culture flask by trypsinization (0.25% trypsin + 0.1% EDTA) and suspended in complete medium.

Cell Viability. Quantitative viability of the 3T3 and HeLa cells in the presence of MNPs was assessed using the MTT and NR assays, as described elsewhere.[58] The first measures metabolic activity in the mitochondria of viable cells,[59] whereas NR accumulates in the lysosomes of viable undamaged cells.[60] 3T3 cells (1×10^5 cells mL^{-1}) and HeLa cells (5×10^4 cells mL^{-1}) were seeded onto a 96-well plate in 100 μL of complete medium. After subculturing for 24 h at 37 °C and 5% CO_2, the medium was replaced with 100 μL of fresh medium supplemented with 5% FCS containing the MLPs in the phospholipid concentration range of 0.08−10 mM (with an iron content ranging from 0.03 to 4 mM). The control group consisted of cells in DMEM supplemented with 5% fetal bovine serum without MLPs. Experiments were carried out in triplicate. After exposure for 24 h to MLPs, PEG-MLPs, or RGD-MLPs, the nanoparticles were removed. Subsequently, 100 μL of MTT solution (1 mg mL^{-1}), previously diluted with DMEM without FCS or phenol red, was added to each well at a final concentration of 0.5 mg mL^{-1}. After 3 h of incubation at 37 °C, the MTT solution was removed by aspiration and 100 μL of dimethyl sulfoxide was added to each well to dissolve the purple formazan crystals. Plates were then placed in a microtiter plate shaker and gently shaken for 10 min at room temperature to achieve complete dissolution. Finally, the absorbance of each well was measured at 550 nm using a Bio-Rad 550 microplate reader. Cell viability was expressed as the percentages of viable cells compared with the survival rates of the control group (untreated cells showed 100% viability). In the NR assay, after incubating cells with MLPs for 24 h, an additional incubation for 3 h was performed with an NR solution (50 μg mL^{-1}) in DMEM without FCS or phenol red. Cells were then washed with PBS, followed by the addition of 100 μL of a solution containing 50% absolute ethanol and 1% acetic acid in distilled water to extract NR. Plates were gently shaken for 10 min to ensure complete dissolution, and the absorbance of the extracted solution was read at 550 nm as above. The effect of each type of MLP was calculated as the percentage of NR uptake by lysosomes compared to that in control (untreated cells). Viability was determined as in the MTT assay.

Flow Cytometry. The interaction between the MLPs and 3T3 or HeLa cells was determined by flow cytometry. 3T3 cells (1×10^5 cells mL^{-1}) and HeLa cells (5×10^4 cells mL^{-1}) were seeded onto 24-well plates in 500 μL of complete medium. The cells were then incubated for 24 h at 37 °C under 5% CO_2. The medium was replaced with 500 μL of fresh DMEM supplemented with 5% FCS containing the MLPs at a phospholipid concentration of 0.6 mM. After 4 h of incubation, the MLPs were removed and the cells were washed three times with PBS and harvested with trypsin/EDTA (100 μL) for 3−5 min at 37 °C under 5% CO_2. Cells were resuspended in 500 μL of fresh DMEM supplemented with 10% FCS and analyzed by flow cytometry using a FACSAria I SORP sorter (Becton Dickinson, San Jose, CA). Excitation of the sample was achieved using a blue laser (488 nm) for forward scatter (FS). A green laser (561 nm) was used to excite Rho present in the bilayer of MLPs, and the red emission (575 ± 12.5 nm) was collected in log modes. Cells were gated by sideward scatter (SS) versus forward scatter (FS) and selected according to their FS/SS signal. Fluorescence measurements were undertaken according to this gate. A minimum of 10 000 (3T3 cells) or 3900 (HeLa cells) gated events were collected and analyzed. Dot blot analysis was performed using the software supplied by the manufacturer. All experiments were repeated twice, but results are presented from a single experiment.

Confocal Microscopy. Cell adhesion and MLP localization in both cell lines were assessed by confocal microscopy using a Leica TCS−SP2 laser scanning confocal microscope (Heidelberg, Germany). The cell membrane was stained with the cell-membrane-impermeable dye Alexa Fluor 488-conjugated WGA in ice-cold PBS for 10 min. The nucleus was stained using membrane-permeable dye Hoechst 33342 (L7528, Invitrogen). Cells were washed three times with ice-cold PBS, and the coverslips with the cells were mounted on glass slides onto ProLong Gold antifade reagent. For every sample, 15-z scans (horizontal cross section of a cell at a particular z height) were taken at a 0.25 μm z-step height to cover the entire height of the cell. On the confocal images, liposomes are shown in red, the cell membrane, in green, and the nucleus, in blue.

■ ASSOCIATED CONTENT

Supporting Information

The Supporting Information is available free of charge on the ACS Publications website at DOI: 10.1021/acsomega.7b00778.

Half-minimal inhibitory concentration of the nanoparticulate systems, cellular toxicity on 3T3 and HeLa cells, and gating strategy for flow cytometry analysis (PDF)

■ AUTHOR INFORMATION

Corresponding Author

*E-mail: joanestelrich@ub.edu. Phone: +34 934 024 559.

ORCID

Maria Antònia Busquets: 0000-0002-6232-9886

DOI: 10.1021/acsomega.7b00778
ACS Omega 2017, 2, 6544−6555

Notes

The authors declare no competing financial interest.

■ ACKNOWLEDGMENTS

The authors thank the project 2014SGR227 of the Generalitat of Catalunya. They also acknowledge Dr. S. Estradé from the Department of Engineering: Section of Electronics, Faculty of Physics, University of Barcelona for the TEM, HRTEM and HAADF images.

■ ABBREVIATIONS

CHOL, cholesterol; DMPC, 1,2-dimyristoyl-*sn*-glycero-3-phosphocholine; DSPE-PEG, 1,2-distearoyl-*sn*-glycero-3-phosphoethanolamine-*N*-[maleimide (polyethylene glycol)-2000] (ammonium salt) (DSPE-Mal-PEG-2000); EPR, enhanced permeability and retention; FCS, fetal calf serum; FS, forward scatter; IC_{50}, half-maximal inhibitory concentration; HAADF, high angle annular dark field; MLPs, magnetoliposomes; MNPs, magnetic nanoparticles; MTT, 3-4,5-dimethylthiazol-2-yl)-2,5-diphenyltetrazoliumbromide; NR, neutral red; PCS, photon correlation spectroscopy; PEG, poly(ethylene glycol); PEG, 1,2-distearoyl-*sn*-glycero-3-phosphoethanolamine-*N*-[methoxy(polyethylene glycol)-2000] (ammonium salt); RGDc, cyclic arginine-glycine-aspartate peptide; Rho, rhodamine B; SS, sideward scatter; WGA, wheat germ agglutinin

■ REFERENCES

(1) Torchilin, V. P. Drug targeting. *Eur. J. Pharm. Sci.* **2000**, *11*, S81−S91.
(2) Zhang, L.; Gu, F. X.; Chan, J. M.; Wang, A. Z.; Langer, R. S.; Farokhzad, O. C. Nanoparticles in medicine: Therapeutic applications and developments. *Clin. Pharm. Ther.* **2008**, *83*, 761−769.
(3) Reddy, L. H.; Arias, J. L.; Nicolas, J.; Couvreur, P. Magnetic nanoparticles: design and characterization, toxicity and biocompatibility, pharmaceutical and biomedical applications. *Chem. Rev.* **2012**, *112*, 5818−1878.
(4) Avilés, M. O.; Ebner, A. D.; Ritter, J. A. In vitro study of magnetic particle seeding for implant assisted-magnetic drug targeting. *J. Magn. Magn. Mater.* **2008**, *320*, 2640−2646.
(5) Kong, S. D.; Zhang, W. Z.; Lee, J. H.; Brammer, K.; Lal, R.; Karin, M.; Jin, S. Magnetically vectored nanocapsules for tumor penetration and remotely switchable on-demand drug release. *Nano Lett.* **2010**, *10*, 5088−5092.
(6) García-Jimeno, S.; Escribano, E.; Queralt, J.; Estelrich, J. External magnetic field-induced selective biodistribution of magnetoliposomes in mice. *Nanoscale Res. Lett.* **2012**, *7*, No. 452.
(7) Hynes, R. O. Integrins: A family of cell surface receptors. *Cell* **1987**, *48*, 549−554.
(8) Plow, E. F.; Haas, T. A.; Zhang, L.; Loftus, J.; Smith, J. W. Ligand binding to integrins. *J. Biol. Chem.* **2000**, *275*, 21785−21788.
(9) Hölig, P.; Bach, M.; Völkel, T.; Nahde, T.; Hoffmann, S.; Müller, R.; Kontermann, R. E. Novel RGD lipopeptides for the targeting of liposomes to integrin-expressing endothelial and melanoma cells. *Protein Eng., Des. Sel.* **2004**, *17*, 433−441.
(10) Pierschbacher, M. D.; Ruoslahti, E. Influence of stereochemistry of the sequence Arg-Gly-Asp-Xaa on binding specificity in cell adhesion. *J. Biol. Chem.* **1987**, *262*, 17294−17298.
(11) Temming, K.; Schiffelers, R. M.; Molema, G.; Kok, R. J. RGD-based strategies for selective delivery of therapeutics and imaging agents to the tumour vasculature. *Drug Resist. Updates* **2005**, *8*, 381−402.
(12) Bogdanowich-Knipp, S. J.; Chakrabarti, S.; Williams, T. D.; Dillman, R. K.; Siahaan, T. J. Solution stability of linear vs. cyclic RGD peptides. *J. Pept. Res.* **1999**, *53*, 530−541.
(13) Zitzmann, S.; Ehemann, V.; Schwab, M. Arginine-glycine-aspartic acid (RGD)-peptide binds to both tumor and tumor-endothelial cells in vivo. *Cancer Res.* **2002**, *62*, 5139−5143.
(14) Maurer, N.; Fenske, D. B.; Cullis, P. R. Developments in liposomal drug delivery systems. *Expert. Opin. BIol. Ther.* **2001**, *1*, 923−947.
(15) Lasic, D. D. Recent developments in medical applications of liposomes: sterically stabilized liposomes in cancer therapy and gene delivery in vivo. *J. Controlled Release* **1997**, *48*, 203−222.
(16) Maeda, H.; Wu, J.; Matsumura, Y.; Hori, K.; et al. Tumor vascular permeability and the EPR effect in macromolecular therapeutics: A review. *J. Controlled Release* **2000**, *65*, 271−284.
(17) Lasic, D. D. Doxorubicin in sterically stabilized liposomes. *Nature* **1996**, *380*, 561−562.
(18) Torchilin, V. Tumor delivery of macromolecular drugs based on the EPR effect. *Adv. Drug Delivery Rev.* **2011**, *63*, 131−135.
(19) Fröhlich, E. The role of surface charge in cellular uptake and cytotoxicity of medical nanoparticles. *Int. J. Nanomed.* **2012**, *7*, 5577−5591.
(20) Stümpel, J.; Vaz, W. L. C.; Hallman, D. An X-ray diffraction and differential scanning calorimetric study on the effect of sucrose on the properties of phosphatidylcholine bilayers. *Biochim. Biophys. Acta* **1985**, *821*, 165−168.
(21) Moghaddam, B.; McNeil, S. E.; Zheng, Q.; Mohammed, A. R.; Perrie, Y. Exploring the correlation between lipid packing in lipoplexes and their transfection efficacy. *Pharmaceutics* **2011**, *3*, 848−864.
(22) Armengol, X.; Estelrich, J. Physical stability of different liposome compositions obtained by extrusion method. *J. Microencapsulation* **1995**, *12*, 525−535.
(23) Hansen, C. B.; Kao, G. Y.; Moase, E.; Zalipsky, S.; Allen, T. M. Attachment of antibodies to sterically stabilized liposomes: evaluation, comparison and optimization of coupling procedures. *Biochim. Biophys. Acta* **1995**, *1239*, 133−144.
(24) Domenech, M.; Marrero-Berrios, I.; Torres-Lugo, M.; Rinaldi, C. Lysosomal membrane permeabilization by targeted magnetic nanoparticles in alternating magnetic fields. *ACS Nano* **2013**, *7*, 5091−5101.
(25) Demirgöz, D.; Garg, A.; Kokkoli, E. PR_b-targeted PEGylated liposomes for prostate cancer therapy. *Langmuir* **2008**, *24*, 13518−13524.
(26) Zhao, H.; Wang, J.-C.; Sun, Q.-S.; Luo, C.-L.; Zhang, Q. RGD-based strategies for improving antitumor activity of paclitaxel-loaded liposomes in nude mice xenografted with human ovarian cancer. *J. Drug Targeting* **2009**, *17*, 10−18.
(27) Liu, X. Y.; Ruan, L.; Mao, W.; Wang, J.-Q.; Shen, Y.; Sui, M. Preparation of RGD-modified long circulating liposome loading matrine, and its in vitro anti-cancer effects. *Int. J. Med. Sci.* **2010**, *7*, 197−208.
(28) Soenen, S. J. H.; Brisson, A. R.; Jonckheere, E.; Nuytten, N.; Tan, S.; Himmelreich, U.; De Cuyper, M. The labeling of cationic iron oxide nanoparticle-resistant hepatocellular carcinoma cells using targeted magnetoliposomes. *Biomaterials* **2011**, *32*, 1748−1758.
(29) Su, W.; Wang, H.; Wang, S.; Liao, Z.; Kang, S.; Peng, Y.; Han, L.; Chang, J. PEG/RGD-modified magnetic polymeric liposomes for controlled drug release and tumor cell targeting. *Int. J. Pharm.* **2012**, *426*, 170−181.
(30) Yan, C.; Wu, Y.; Feng, J.; Chen, W.; Liu, X.; Hao, P.; Yang, R.; Zhang, J.; Lin, B.; Xu, Y.; Liu, R. Anti-$\alpha v\beta 3$ antibody guided three-step pretargeting approach using magnetoliposomes for molecular magnetic resonance imaging of breast cancer angiogenesis. *Int. J. Nanomed.* **2013**, *38*, 245−255.
(31) Barczyk, M.; Carracedo, S.; Gullberg, D. Integrins. *Cell Tissue Res.* **2010**, *339*, 269−280.
(32) De Meyer, F.; Smit, B. Effect of cholesterol on the structure of a phospholipid bilayer. *Proc. Natl. Acad. Sci. U.S.A.* **2009**, *106*, 3654−3658.
(33) Garbuzenko, O.; Barenholz, Y.; Priev, A. Effect of grafted PEG on liposome size and on compressibility and packing of lipid bilayer. *Chem. Phys. Lipids* **2005**, *135*, 117−129.
(34) Patil, U. S.; Adireddy, S.; Mandava, J. A.; Lee, B. R.; Chrisey, D. B.; et al. In vitro/in vivo toxicity evaluation and quantification of iron oxide nanoparticles. *Int. J. Mol. Sci.* **2015**, *16*, 24417−24450.
(35) Soenen, S. J.; Nuytten, N.; De Meyer, S. F.; De Smedt, S. C.; De Cuyper, M. High intracelular iron oxide nanoparticle concentrations

DOI: 10.1021/acsomega.7b00778
ACS Omega 2017, 2, 6544−6555

affect cellular cytoskeleton and focal adhesion kinase-mediated signaling. *Small* **2010**, *6*, 832−842.
(36) Pisanic, T. R., 2nd; Jin, S.; Shubayev, V. I. Iron oxide magnetic magnetic nanoparticle toxicity: incidence and mechanisms. In *Nanotoxicity: in vivo and in vitro models to health risk*; Sahu, S., Casciano, D., Eds.; John Wiley and Sons: Chichester, 2009; pp 397−425.
(37) Soenen, S. J. H.; Himmelreich, U.; Nuytten, N.; De Cuyper, M. Cytotoxic effects of iron oxide nanoparticles and implications for safety in cell labelling. *Biomaterials* **2011**, *32*, 195−205.
(38) Díaz, B.; Sánchez-Espinel, C.; Arruebo, M.; Faro, J.; de Miguel, E.; Magadán, S.; Yagüe, C.; Fernández-Pacheco, R.; Ibarra, M. R.; Santamaría, J.; González-Fernández, A. Assessing methods for blood cell cytotoxicity responses to inorganic nanoparticles and nanoparticle aggregates. *Small* **2008**, *4*, 2025−2034.
(39) Urbán, P.; Estelrich, J.; Cortés, A.; Fernàndez-Busquets, X. A nanovector with complete discrimination for targeted delivery to *Plasmodium falciparum*-infected versus non-infected red bloods cells in vitro. *J. Controlled Release* **2011**, *151*, 202−211.
(40) Oh, N.; Park, J.-O. Endocytosis and exocytosis of nanoparticles in mammalian cells. *Int. J. Nanomed.* **2014**, *9*, 51−63.
(41) Ivensen, T. G.; Skotland, T.; Sandvig, K. Endocytosis and intracellular transport to nanoparticles: present knowledge and need for future studies. *Nano Today* **2011**, *6*, 176−185.
(42) Oba, M.; Fukushima, S.; Kanayama, N.; Aoyagi, K.; Nishiyama, N.; Koyama, H.; Kataoka, K. Cyclic RGD peptide-conjugated polyplex micelles as a targetable gene delivery system directed to cells possessing $\alpha_V\beta_3$ and $\alpha_V\beta_5$ integrins. *Bioconjugate Chem.* **2007**, *18*, 1415−1423.
(43) Danhier, F.; Vroman, B.; Lecouturier, N.; Crokart, N.; Pourcelle, V.; Freichels, H.; Jérôme, C.; Marchand-Brynaert, J.; Feron, O.; Préat, V. Targeting of tumor endothelium by RGD-grafted PLGA-nanoparticles loaded with paclitaxel. *J. Controlled Release* **2009**, *140*, 166−173.
(44) Miller, C. R.; Bondurant, B.; McLean, S. D.; McGovern, K. A.; O'Brien, D. F. Liposome-cell interactions in vitro: Effect of liposome surface charge on the binding and endocytosis of conventional and sterically stabilized liposomes. *Biochemistry* **1998**, *37*, 12875−12883.
(45) Villanueva, A.; Cañete, M.; Roca, A. G.; Calero, M.; Veinemillas-Verdaguer, S.; Serna, C. J.; Morales, M. d. P.; Miranda, R. The influence of surface functionalization of the enhanced internalization of magnetic nanoparticles in cancer cells. *Nanotechnology* **2009**, *20*, No. 115103.
(46) Mishra, S.; Webster, P.; Davis, M. E. PEGylation significantly affects cellular uptake and intracellular trafficking of non-viral gene delivery particles. *Eur. J. Cell Biol.* **2004**, *83*, 97−111.
(47) Hatakeyama, H.; Akita, H.; Kogure, K.; Oishi, M.; Nagasaki, Y.; Kihira, Y.; Ueno, M.; Kobayashi, H.; Kikuchi, H.; Harashima, H. Development of a novel system in gene delivery system for cancer therapy with a tumor-specific cleavable PEG-lipid. *Gene Ther.* **2007**, *14*, 68−77.
(48) Hama, S.; Itakura, S.; Nakai, M.; Nakayama, K.; Morimoto, S.; Suzuki, S.; Kogure, K. Overcoming the polyethylene glycol dilemma via pathological environment-sensitive change of the surface property of nanoparticles for cellular entry. *J. Controlled Release* **2015**, *206*, 67−74.
(49) Walczyk, D.; Baldelli Bombelli, F.; Monopoli, M. P.; Lynch, I.; Dawson, K. A. What the cell "sees" in Bionanoscience. *J. Am. Chem. Soc.* **2010**, *132*, 5761−5766.
(50) Guo, Z.; He, B.; Jin, H.; Zhang, H.; Dai, W.; Zhang, L.; et al. Targeting efficiency of RGD-modified nanocarriers with different ligand intervals in response to integrin $\alpha_V\beta$3 clustering. *Biomaterials* **2014**, *35*, 6106−6117.
(51) Ruoslahti, E.; Bhatia, S. N.; Sailor, M. J. Targeting of drugs and nanoparticles to tumors. *J. Cell Biol.* **2010**, *188*, 759−768.
(52) Pozzi, D.; Colapicchioni, V.; Caracciolo, G.; Piovesana, S.; Capriotti, A. L.; Palchetti, S.; De Grossi, S.; Riccioli, A.; Amenitsch, H.; Laganà, A. Effect of polyethyleneglycol (PEG) chain length on the bio-nano-interactions between PEGylated lipid nanoparticles and biological fluids: from nanostructure to uptake in cancer cells. *Nanoscale* **2014**, *6*, 2782−2792.
(53) Torchilin, V. P.; Omelyanenko, V. G.; Papisov, M. I.; Trubetskoy, V. S.; Herron, J. N.; Gentry, C. A.; et al. Poly(ethylene glycol) on the liposome surface: on the mechanism of polymer-coated liposome longevity. *Biochim. Biophys. Acta* **1994**, *1195*, 11−20.
(54) Torchilin, V. P.; Papisov, M. I. Why do Polyethylene Glycol-Coated Liposomes Circulate So Long?: Molecular Mechanism of Liposome Steric Protection with Polyethylene Glycol: Role of Polymer Chain Flexibility. *J. Liposome Res.* **1994**, *4*, 725−739J.
(55) García-Jimeno, S.; Estelrich, J. Ferrofluid based on polyethylene glycol-coated iron oxide nanoparticles: Characterization and properties. *Colloid Surf., A* **2013**, *420*, 74−81.
(56) Steward, J. C. M. Colorimetric determination of phospholipids with ammonium ferrothiocyanate. *Anal. Biochem.* **1980**, *104*, 10−14.
(57) Kiwada, H.; Sato, J.; Yamada, S.; Kato, Y. Feasibility of magnetic liposomes as a targeting device for drugs. *Chem. Pharm. Bull.* **1986**, *34*, 4253−4258.
(58) Kwasigroch, B.; Escribano, E.; Morán, M. C.; Queralt, J.; Busquets, M. A.; Estelrich, J. Oil-in-water nanoemulsions are suitable for carrying hydrophobic compounds: Indomethacin as a model of anti-inflammatory drug. *Int. J. Pharm.* **2016**, *515*, 749−756.
(59) Mosmann, T. Rapid colorimetric assay for cellular growth and survival: application to proliferation and cytotoxicity assays. *J. Immunol. Methods* **1983**, *65*, 55−63.
(60) Borenfreund, E.; Puerner, J. A. Toxicity determined in vitro by morphological alterations and neutral red absorption. *Toxicol. Lett.* **1985**, *24*, 119−124.

DOI: 10.1021/acsomega.7b00778
ACS Omega 2017, 2, 6544−6555